Molecular Catalysis 524 (2022) 112315

Contents lists available at ScienceDirect

Molecular Catalysis

journal homepage: www.journals.elsevier.com/molecular-catalysis

Editor's choice paper

Stereodivergent evolution of *Kp*ADH for the asymmetric reduction of diaryl ketones with *para*-substituents

Jiacheng Zhang, Jieyu Zhou, Guochao Xu *, Ye Ni *

Key Laboratory of Industrial Biotechnology, Ministry of Education, School of Biotechnology, Jiangnan University, Wuxi 214122, Jiangsu, China

ARTICLE INFO

Keywords:
Alcohol dehydrogenase
Diaryl ketone
Stereeoselectivity
Stereoocomplementary
Chiral alcohol

ABSTRACT

*Kp*ADH is a promising biocatalyst for the synthesis of chiral bulky-bulky alcohols. Substrate specificity toward diaryl ketone substrates with different substituents at phenyl group was investigated. The results reveal that the *para*-position of diaryl ketones plays important role in manipulating the stereoselectivity of *Kp*ADH. Two vital residues, E214 and T215, were identified through single-point mutagenesis, and saturation mutagenesis was performed to evaluate their contributions to the stereoselectivity. Furthermore, stereodivergent evolution of *Kp*ADH was achieved through combinatorial mutagenesis. Among them, E214I/T215S/S237A (ISA) and F161V/S196G/E214G (VGG) exhibited *e.e.* values of >99% (*S*) and 99% (*R*) toward [4-(trifluoromethyl)phenyl]-2-pyridinylmethanone (**5a**), and *e.e.* values of >99% (*S*) and 98% (*R*) toward (4-methylphenyl)-2-pyridinylmethanone (**6a**), respectively. Kinetic characterization and interaction analysis further prove that the eliminated side-chain collision and enhanced electrostatic interactions are mainly responsible for the increased catalytic efficiency and stereoselectivity. This study provides beneficial mutants with complementary stereoselectivity toward diaryl ketones with *para*-substituents and also provides guidance for the engineering of homologous alcohol dehydrogenases toward bulky-bulky ketones.

1. Introduction

Asymmetric reduction utilizing chemo- or bio-catalysts is one of the most widely implemented reactions for the synthesis of chiral secondary alcohols, which are important building blocks of pharmaceuticals, agrochemicals, materials, etc [1–3]. Recently, the importance of bioreduction catalyzed by alcohol dehydrogenases (ADHs) or ketoreductases (KREDs) has drawn growing attention, due to the advantages of 100% theoretical yield, high atomic economy, mild conditions, and environmental friendliness [4–6]. Many ADHs and KREDs have been developed and evaluated at industrial scale [7]. However, due to their sophisticated structure of active centers, ADHs often display strict substrate spectrum. There is a continuous demand to develop novel ADHs with high activity and stereoselectivity toward prochiral ketones with non-natural structure.

In the asymmetric reduction of prochiral ketones, ADHs follow Prelog or anti-Prelog rule to produce (*R*)- or (*S*)-secondary alcohols [8–11], which usually exhibit different pharmaceutical effects or characteristics. For example, ethyl (*S*)-4-chloro-3-hydroxybutanoate is the key chiral intermediate for the synthesis of HMG-CoA reductase inhibitor Atorvastatin, while (*R*)-4-chloro-3-hydroxybutanoate is applied to the synthesis of L-Carnitine [12–14]. Therefore, it is of industrial importance to develop stereocomplementary ADHs for the synthesis of both enantiomers of secondary alcohols. Moreover, the development of ADHs with stereocomplementary substrate binding pockets is of special interest for elucidating the molecular mechanism underlying the enantioselective discrimination and recognition of *pro*-R and *pro*-S substrates [15].

Chiral diaryl alcohols are a class of important chemicals, which are widely used in the synthesis of a variety of drugs such as antihistamines, diuretics, asthma drugs, antiepileptic drugs and antidepressants [16, 17]. Among various synthetic approaches, asymmetric reduction of prochiral ketone employing ADHs is the most promising one. However, due to the large steric hindrance and highly symmetric structure of diaryl ketones, only a few ADHs have been reported to possess high catalytic activity and stereoselectivity [18–20]. To further improve the catalytic efficiency and stereoselectivity, directed evolution and semi-rational mutagenesis were performed. A zinc-dependent alcohol dehydrogenase was identified from *Thermoanaerobacer brockii* (*Tb*SADH) with capability in the asymmetric reduction of diaryl ketones, however, with unmeasurably low activity [21]. The stereoselectivity

* Corresponding authors.
E-mail addresses: guochaoxu@jiangnan.edu.cn (G. Xu), yni@jiangnan.edu.cn (Y. Ni).

https://doi.org/10.1016/j.mcat.2022.112315
Received 7 March 2022; Received in revised form 13 April 2022; Accepted 15 April 2022
Available online 29 April 2022

and activity toward (4-chlorophenyl)-2-pyridinylmethanone (CPMK) were improved through conformational dynamic of *Kp*ADH [22] and proline-induced loop engineering for *Tb*SADH [23]. However, the application and the stereo-preference of *Tb*SADH toward other diaryl ketones with different substituents were unexplored. The influence of substitution at different positions of diaryl ketones remains to be elucidated.

Previously, an NADPH-dependent alcohol dehydrogenase *Kp*ADH has been identified from *Kluyveromyces polysporus*. *Kp*ADH displayed moderate stereoselectivity of 82% (*R*) and the highest catalytic efficiency (k_{cat}/K_M of 17.9 $s^{-1}\cdot mM^{-1}$) toward CPMK among all the reported ADHs or KREDs [24]. To modulate its stereoselectivity, protein engineering of *Kp*ADH has been performed to obtain mutants with strict (*R*)- and (*S*)-preference toward CPMK [20,22,24-26]. However, the effect of various substituents of diaryl ketones on the stereoselectivity of ADHs remains unclear.

To explore the stereochemistry of *Kp*ADH, several CPMK analogues with substituents of different size, electrostatic property, and positions at phenyl group were synthesized in this study. The *para*-position of phenyl group was demonstrated to be critical to the stereoselectivity of *Kp*ADH. Furthermore, structure-guided rational engineering of *Kp*ADH was conducted for stereodivergent evolution of its stereoselectivity toward CPMK analogues, in which two stereocomplementary mutants were obtained. Deconvolution analysis was also performed to elucidate the contributions of key residues on the stereo-preference. This study demonstrates the potential of *Kp*ADH in the enantioselective synthesis of chiral diaryl alcohols with different substituents and pharmaceutical values.

2. Material and methods

2.1. Chemicals, strains and plasmids

KOD polymerase used for PCR was purchased from Toyobo Co., Ltd. Quickcut *Dpn*I was bought from Takara Co., Ltd. Tryptone and yeast extract were purchased from Oxoid Co. Ltd. Chemicals of analytical grade were bought from Aladdin and Sinopharm. (3-chlorophenyl)-2-pyridinylmethanone (**2a**), (2-chlorophenyl)-2-pyridinylmethanone (**3a**), (4-bromophenyl)-2-pyridinylmethanone (**4a**), [4-(trifluoromethyl)phenyl]-2-pyridinylmethanone (**5a**), and (4-methylphenyl)-2-pyridinylmethanone (**6a**) were synthesized in this study using the method as shown in Supplementary Materials. *E. coli* BL21 (DE3) was used for protein expression using Luria–Bertani (LB) medium (5 $g\cdot L^{-1}$ yeast extract, 10 $g\cdot L^{-1}$ tryptone, and 10 $g\cdot L^{-1}$ NaCl).

Recombinant plasmid pET28a-*Kp*ADH coding for alcohol dehydrogenase from *Kluyveromyces polyspora* was constructed in the previous study and stored in our lab [24]. Primers used for site-directed mutagenesis were designed by SnapGene and synthesized at Tianlin Company (Wuxi, China). Glucose dehydrogenase (*Bm*GDH) [27] for cofactor regeneration was derived from *Bacillus megatherium*.

2.2. Site-Directed Mutagenesis

Mutagenesis was performed by whole-plasmid PCR with pET28a-*Kp*ADH as template and primers listed in **Table S1**, employing PCR mixture: 2.0 μL 10× KOD buffer, 0.5 μL template, 0.4 μL primers (10 μM each), 2.0 μL dNTPs (2 mM each), 1.2 μL $MgSO_4$ (25 mM), 13.3 μL ddH_2O and 0.2 μL KOD. The PCR procedure was set as: pre-denaturation at 98°C for 2 min, 25 cycles of denaturation at 98°C for 15 s, annealing at 49°C for 15 s and extension at 68°C for 3 min, further extension at 68°C for 10 min. The resultant PCR products were confirmed by electrophoresis. Then, 2 μL PCR product was transferred to a new EP tube, followed by addition of 2.5 μL 10 × Quickcut buffer, 20 μL ddH_2O, and 0.5 μL *Dpn*I. The mixture was incubated at 37°C for 1 h to remove the template plasmids. Finally, 10 μL digestion mixture was transformed into *E. coli* BL21(DE3) competent cells by $CaCl_2$-mediated chemical transformation. After grew on LB solid medium supplemented with 50 $\mu g\cdot mL^{-1}$ kanamycin at 37°C for 12 h, positive clones were evaluated and identified by DNA sequencing (Tianlin Company, Wuxi, China). Finally, the recombinant plasmid was extracted by AxyPrep Plasmid Miniprep Kit.

2.3. Expression and purification of KpADH mutants

Positive clones were picked and inoculated into LB medium supplemented with kanamycin (50 $\mu g\cdot mL^{-1}$), and cultivated at 37°C and 180 rpm for 12 h. Then, the culture was transferred into 40 mL LB medium in 250 mL flasks with 1% (v/v) inoculum. When the OD_{600} reached 0.6-0.8, 0.2 mM IPTG was added for gene expression at 25°C and 180 rpm for 12−14 h. The cells were collected by centrifugation at 4°C and 8000 rpm for 15 min, and re-suspended with 10 mL A buffer (20 mM phosphate buffer solution (PBS) pH 7.4, 500 mM NaCl, 20 mM imidazole), disrupted by homogenizer (AH-BASICII, ATS Co., Ltd). After centrifugation at 4°C and 8000 rpm for 30 min, the crude extract was purified by nickel affinity chromatography and eluted with gradient concentrations of imidazole. The purified enzymes were verified by SDS-PAGE, and concentrated and stored at –80°C for further use.

2.4. Activity assay

General protocol for determination of enzyme activity was determined by monitoring the absorbance changes of NADPH at 340 nm with molar extinction coefficient of 6220·L·$mol^{-1}\cdot cm^{-1}$. The reaction mixture contains 1 mM substrate, 1 mM NADPH in PBS buffer (100 mM, pH 7.0), and 10 μL enzyme solution with appropriate concentration at 30°C. One unit of activity is defined as the amount of enzyme that catalyzed the oxidation of 1 μmol NADPH per minute under above mentioned conditions.

2.5. Reaction system and product extraction

Reaction system (2 mL) contains 200 μL cell-free extract (approximately 0.6 mg protein), 1 $U\cdot mL^{-1}$ glucose dehydrogenase, 15 mM glucose, 10 mM substrate, 1 mM $NADP^+$ in PBS buffer (100 mM, pH 7.0). The reaction mixture was incubated at 30°C and 180 rpm overnight. At different time intervals, samples were withdrawn from the reaction mixture and extracted with equal volume of ethyl acetate. The organic phase was isolated and dried over anhydrous Na_2SO_4. After evaporation, the mobile phase was added to dissolve the samples for chiral HPLC analysis. After the reaction was complete, equal volume of ethyl acetate was added to extract product for at least three times. The organic phase was isolated by centrifugation at 8000 rpm for 15 min and dried over anhydrous Na_2SO_4. Finally, the organic phase was evaporated in vacuum.

2.6. HPLC analysis of conversion and stereoselectivity

The conversion ratio and stereoselectivity of *Kp*ADH and mutants were determined using the Agilent 1100 equipped with a Chiralcel AD-H column or a Chiralcel OB-H column (0.46 mm × 250 mm × 5 μm, Diacel, Japan). OB-H was employed at 254 nm using hexane/ethanol (95:5, v/v) as eluent at a flow rate of 1.0 $mL\cdot min^{-1}$ and 30°C, OD-H was employed at 254 nm using hexane/ isopropanol (90:10, v/v) as eluent at a flow rate of 1.0 $mL\cdot min^{-1}$ and 30°C. Detailed conditions for stereoselectivity analysis and retention times of (*R*)- and (*S*)-alcohols could be found in Supplementary Materials.

2.7. Enzyme kinetics

Kinetic parameters of purified *Kp*ADH mutants were determined employing above mentioned activity assay method. The reactions contained final concentrations of substrates varied from 0.05 mM to 10 mM, 1 mM NADPH, and appropriate amount of purified enzymes.

Concentrations of **5a** and **6a** varied from 0.05 mM to 5 mM. All assay was performed in triplicate. The K_M, V_{max}, and k_{cat} values were calculated according to the Lineweaver-Burk plot.

Substrate specificities of purified *Kp*ADH mutants toward **1a, 5a**, and **6a** were analyzed by determining the specific activities using the above described method. The final concentration of each substrate was 1.0 mM. All the activity was measured in triplicate.

2.8. Structural analysis and Mutant modeling

Crystal structure of *Kp*ADH in complex with $NADP^+$ was deposited in PDB under accession No. 5Z2X. Models of VGG and ISA were constructed using online homology modeling tool and evaluated by PROCHECK. Substrates were docked into the active center of *Kp*ADH mutants using Autodock VINA to construct the initial conformation for interaction analysis. Structural alignment and interactions between substrates and *Kp*ADH mutants were analyzed using Discovery studio, the results were viewed in Pymol.

3. Results and Discussion

3.1. Effect of para-substitution on the enantioselectivity of KpADH

*Kp*ADH was identified from *Kluveromyces polysporus*, and displayed high activity toward bulky-bulky substrates such as (4-chlorophenyl)-2-pyridinylmethanone (**1a**) [20,22,24-26]. In order to further explore the application potential of *Kp*ADH in the synthesis of chiral bulky-bulky alcohols, the substrate spectrum of *Kp*ADH was investigated Several prochiral bulky-bulky ketones with similar structure as **1a**, including (3-chlorophenyl)-2-pyridinylmethanone (**2a**), (2-chlorophenyl)-2-pyridinylmethanone (**3a**), (4-bromophenyl)-2-pyridinylmethanone (**4a**), [4-(trifluoromethyl)phenyl]-2-pyridinylmethanone (**5a**) and (4-methylphenyl)-2-pyridinylmethanone (**6a**), were selected for specificity analysis. Substrates **1a** to **5a** contain an electron-withdrawing group, while substrate **6a** has an electron-donating group at the *para* position of the phenyl group.

The relative activity and *e.e.* values of *Kp*ADH were shown in Fig. 1. For substrate **1a**–**3a** with chloro-group at *para, meta* or *ortho* position of the phenyl group and same 2'-pyridyl group, the relative activities decreased from 17.6 U·mg^{-1} to 4.76 U·mg^{-1} and 0.08 U·mg^{-1}, due to the increased hindrance at *meta* and *ortho* positions which are unfavorable for stabilizing at substrate binding pocket. Similar trend was also observed in enantioselectivity with *e.e.* values toward **1a, 2a** and **3a** decreasing from 82% (*R*) to 57% (*R*) and 7% (*S*). All above indicated the important role of *para* chloro-group at phenyl group in influencing the catalytic efficiency of *Kp*ADH.

The relative activity toward **4a** was merely 1.76 U·mg^{-1}, despite the similar properties of chloro- and bromo-group. The bromo-group is larger than the chloro-group, indicating the larger steric hindrance of **4a** compared with **1a**. However, it should be noted that the *e.e.* value toward **4a** was 96% (*R*), much higher than 82% (*R*) of **1a**, which might be attributed to the distinction between phenyl group and pyridyl group of **4a**. Therefore, *Kp*ADH could easily discriminate the *pro*-R and *pro*-S conformation of **4a** and exhibited higher stereoselectivity. To further explore the role of electronegativity in influencing the stereoselectivity, substrate **5a** with electron-withdrawing CF_3-group and substrate **6a** with electron-donating CH_3-group were investigated. The activities toward **5a** and **6a** decreased to only 0.18 U·mg^{-1} and 1.23 U·mg^{-1} respectively, compared with that of **1a**, which can be attributed to the significantly increased steric hindrance. CF_3- and CH_3-group are similar in size, and are much larger than the Cl-group. Stereoselectivity analysis revealed that *Kp*ADH displayed (*S*)-preference, with *e.e.* value of 49% (*S*) toward **5a** and 83% (*S*) toward **6a**. Although there are electron-withdrawing groups at the *para* position of **1a** and **5a**, distinct stereoselectivities were observed, indicating their different binding conformations. Based on results of **5a** and **6a**, the steric hindrance plays more important role in determining the stereoselectivity compared with electronegativity. Substrate with strong electron-donating group such as methoxy, was also tested with *Kp*ADH-WT, while no detectable activity was determined. These results demonstrate that the para position of the phenyl group is critical to the enantioselectivity of *Kp*ADH, which is consistent with previous study [28]. Inspired by this interesting phenomenon of *para* substitution of **5a** and **6a**, protein engineering of *Kp*ADH was performed to explore the mechanism in the manipulation of stereoselectivity.

3.2. Identification of key residues in determining the stereoselectivity of KpADH

In our previous study [20,22,24,25], residues Q136, F161, S196, E214, T215, and S237 play important roles in the stereoselectivity of *Kp*ADH toward **1a**. Therefore, site-directed mutagenesis of these

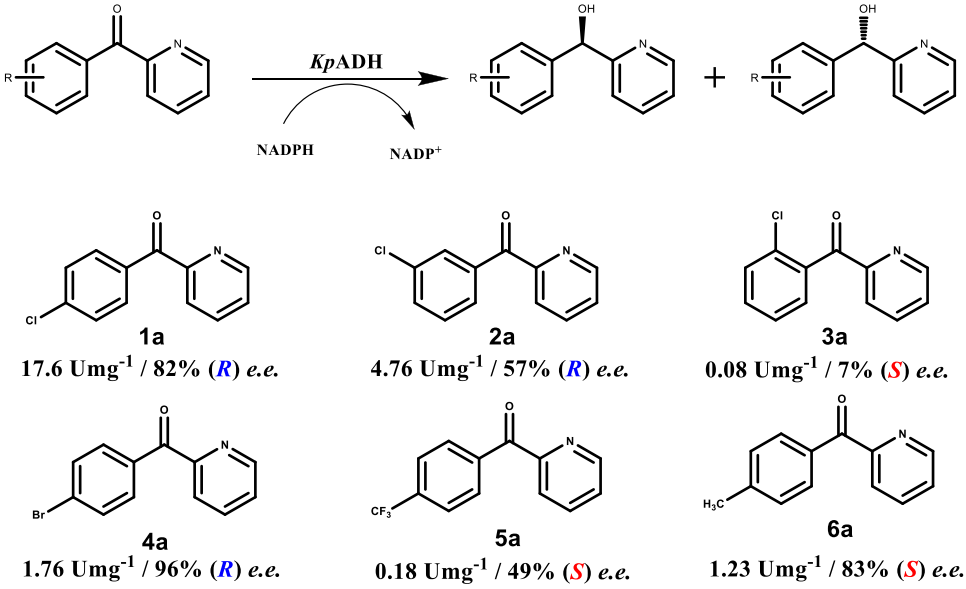

Fig. 1. Asymmetric reduction of bulky prochiral ketones (**1a**-**6a**) to corresponding alcohols catalyzed by *Kp*ADH.

residues was performed. The stereoselectivity of all the mutants toward **1a, 5a**, and **6a** was shown in Table 1. For substrate **1a**, most single mutants produced alcohol products with the same configuration, except for E214G with 7% (*S*). Mutants E214F, T215S, and S237A displayed increased *e.e.* values of 92%, 92%, and 97% toward **1a** respectively. Mutants Q136N, F161V, S196G, T215V, and S237C exhibited decreased *e.e.* values toward **1a**. For substrate **5a**, mutants E214F, T215S, and S237A showed increased stereoselectivity than the wild type *Kp*ADH (WT), with *e.e.* values of 95%, 90%, and 95% (*S*) respectively. While mutants Q136N, F161V, S196G, E214G, T215V, and S237C produced (*R*)-alcohols which are opposite to that of WT. With regard to substrate **6a**, most of the single-point mutants display (*S*)-preference as WT, and only E214G and S237C displayed (*R*)-preference with *e.e.* value of 21% and 21%. The *e.e.* values of mutants E214F and T215S were 89% and 99%, much higher than 82% of WT.

For **1a, 5a**, and **6a**, E214F exhibited enhanced *e.e.* values and the same stereoselectivity compared with WT, whereas reversed stereoselectivity was observed with E214G. A similar trend was also observed in T215. As a result, E214 and T215 were identified to be key residues in manipulating the stereoselectivity of *Kp*ADH.

To further explore their roles in the stereoselectivity, saturation mutagenesis was conducted at E214 and T215. The stereoselectivity of mutants toward **5a** is illustrated in Fig. 2**A** and Fig. 2**B**. As shown in Fig. 2**A**, E214 mutants showed *e.e.* values ranging from 89% (*R*) of E214G to 95% (*S*) of E214Y toward **5a**. Mutation of E214 into aromatic amino acids including Tyr, Phe, and Trp, and into hydrophobic amino acids such as Val, Leu, Ile, and Met, resulted in significantly increased (*S*)-preference toward **5a**. While mutation of E214 into hydrophilic amino acids, such as Arg and Ser, and small amino acids including Ala and Gly, led into reversed (*R*)-preference. With regard to T215, only mutant T215S exhibited increased stereoselectivity with *e.e.* value of 90% (*S*). Mutation of T215 into polar amino acids such as Lys, Asp, Arg, His, and into hydrophobic amino acids such as Leu and Ile, resulted in reversed (*R*)-selectivity, especially T215R with *e.e.* value of 75% (*R*).

The stereoselectivity of mutants toward **6a** is shown in Fig. 2**C** and Fig. 2**D**. Mutation of E214 into hydrophobic Val, Ile Ala, and aromatic Phe and Tyr resulted in increased (*S*)-preference toward **6a**, while only E214G exhibited reversed (*R*)-preference with *e.e.* value of 21% (*R*), which is similar as substrate **5a**. The highest *e.e.* value of 96% (*S*) toward **6a** was achieved with E214V. Only mutants T215S and T215Y showed increased *e.e.* values of 99% (*S*) and 88% (*S*) respectively. While T215N resulted in reversed *e.e.* value of 3% (*R*).

In summary, E214Y and T215S displayed the highest (*S*)-selectivity in the asymmetric reduction of **5a**, while E214G and T215R gave the highest (*R*)-selectivity. With regard to **6a**, E214V and T215S exhibited the highest (*S*)-selectivity, while reversed (*R*)- preference was obtained with E214G and T215N. These results provide interesting single mutants for further combinatorial evolution for mutants with desirable (*R*)- and (*S*)-selectivity.

Table 1
Enantioselectivity of single mutants toward **1a, 5a**, and **6a**.

Mutant	*e.e.* [%]/(*R*/*S*)		
	1a	5a	6a
WT	82 (*R*)	49 (*S*)	83 (*S*)
Q136N	60 (*R*)	2 (*R*)	16 (*S*)
F161V	66 (*R*)	6 (*R*)	80 (*S*)
S196G	44 (*R*)	20 (*R*)	28 (*S*)
E214G	7 (*S*)	89 (*R*)	21 (*R*)
E214F	92 (*R*)	95 (*S*)	89 (*S*)
T215S	92 (*R*)	90 (*S*)	99 (*S*)
T215V	44 (*R*)	53 (*R*)	20 (*S*)
S237C	26 (*R*)	22 (*R*)	21 (*R*)
S237A	97 (*R*)	95 (*S*)	63 (*S*)

Note:All the conversion ratios were detected to be >99% by HPLC analysis.

3.3. Combinatorial evolution of (S)-mutants toward 5a and 6a

Combinatorial mutagenesis was performed to constructed (*S*)-mutants in the asymmetric reduction of **1a, 5a**, and **6a**. Beneficial single mutants were combined. Among double mutants, E214Y/T215S displayed the highest stereoselectivity toward **5a** with 98% (*S*), while E214I/T215S exhibited the highest stereoselectivity toward **6a** with 99% (*S*). Therefore, triple mutants were constructed based on E214Y/T215S and E214I/T215S. Among all the triple mutants, both E214I/T215S/S237A (designated as ISA) and E214Y/T215S/S237A (designated as YSA) exhibited the highest (*S*)-selectivity of >99% in the asymmetric reduction of **5a** and **6a** (Table 2). Due to the higher catalytic activity of ISA than YSA, ISA was regarded as the best (*S*)-mutant for further study.

3.4. Combinatorial evolution of (R)-mutants toward 5a and 6a

Combinatorial mutagenesis was also performed to obtain (*R*)-mutants. Beneficial mutants with the highest stereoselectivity at resides F161, S196, E214, T215, and S237 were rationally combined to construct double and triple mutants. Among all the double mutants, the stereoselectivity of S196G/E214G toward **5a** was 96% (*R*), higher than 92% (*R*) of E214G/S237C. As a result, triple mutants were constructed based on S196G/E214G, and F161V/S196G/E214G (designated as VGG) displayed the highest *e.e.* value of 99% (*R*) toward **5a**. With regard to **6a**, mutant E214G/S237C exhibited the highest *e.e.* value of 95% (*R*), among all the double mutants. However, triple mutants based on E214G/S237C showed decreased stereoselectivity, such as 79% (*R*) of S196G/E214G/S237C, indicating there might be antagonistic effects. As a result, triple mutants were developed based on S196G/E214G, and mutant VGG displayed the highest stereoselectivity of 98% (*R*) toward **6a**. The stereoselectivity toward **1a, 5a**, and **6a** was summarized in Table 3. The *e.e.* value of VGG toward **1a** was 86% (*S*), ranking the highest among all mutants. Since the triple mutant VGG displayed the highest stereoselectivity, it was selected as the (*R*)-mutant for further study.

3.5. Kinetic parameters

Deconvolution analysis was also performed to understand the contribution of each residue in the (*R*)- and (*S*)-mutants. Kinetic parameters of single, double, and triple mutants were determined and summarized in Table 4. The K_M and k_{cat} values toward **5a** of (*R*)-selective VGG were 0.46 mM and 1.18 s^{-1}, which were similar to those of WT. Among the single mutants, E214G displayed the lowest K_M value of 0.05 mM, indicating the vital role of Gly at 214 in substrate binding. The k_{cat}/K_M of E214G was 51.8 $s^{-1}\cdot mM^{-1}$, much higher than 2.41 $s^{-1}\cdot mM^{-1}$ of WT. The K_M of mutant S196G was 0.66 mM, suggesting reduced binding affinity compared with WT. Hence, double mutant S196G/E214G showed further increased the K_M of 1.31 mM. However, F161V was also favorable for substrate binding, with a lower K_M value of 0.24 mM than 0.44 mM of WT. All above contributed to the balanced binding affinity and catalytic efficiency of VGG toward **5a**. With regard to **6a**, a different phenomenon was observed. Mutants S196G, E214G, and F161V all displayed decreased K_M values, indicating increased binding affinity. Whereas the K_M and k_{cat} values of VGG were 1.59 mM and 9.81 s^{-1}, which were similar to 1.59 mM and 7.29 s^{-1} of WT.

The K_M and k_{cat} values toward **5a** of (*S*)-selective ISA were 0.75 mM and 1.10 s^{-1}, indicating the decreased binding affinity. Based on the deconvolution result, T215S, with a significantly decreased K_M value of 0.07 mM, played more important role in binding affinity, while S237A is not favorable for substrate binding with an increased K_M of 0.84 mM. However, in term of k_{cat}, S237A contributed significantly to the catalytic efficiency with k_{cat} value of 2.76 s^{-1}, much higher than 1.04 s^{-1} of WT, while the k_{cat} of T215S was as low as 0.41 s^{-1}. A similar trend was observed in double mutants. With regard to substrate **6a**, the K_M and k_{cat}

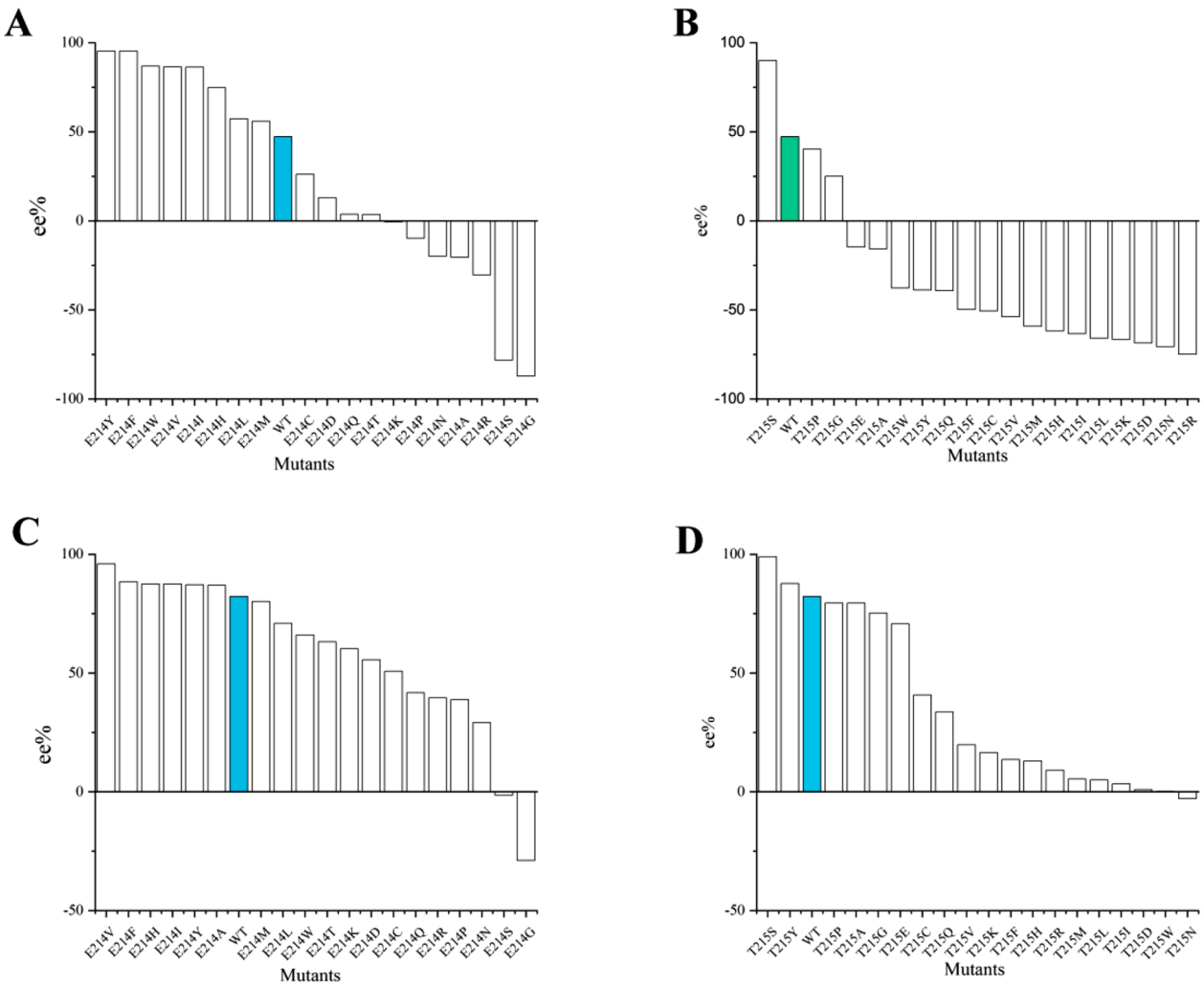

Fig. 2. Stereoselectivity toward **5a** and **6a** of *Kp*ADH mutants constructed by saturation mutagenesis at E214 and T215. (A) E214 mutants toward **5a**; (B) T215 mutants toward **5a**; (C) E214 mutants toward **6a**; (D) T215 mutants toward **6a**. The selectivity of the *e.e.* value show as positive is S.

Table 2
Enantioselectivity of combinatorial mutants with (*S*)-selectivity toward **1a, 5a**, and **6a**.

Mutant	*e.e.* [%]/(*R*/*S*)		
	1a	5a	6a
E214F/T215S	99 (*R*)	98 (*S*)	98 (*S*)
E214H/T215S	98 (*R*)	92 (*S*)	98 (*S*)
E214I/T215S	99 (*R*)	96 (*S*)	99 (*S*)
E214Y/T215S	98 (*R*)	98 (*S*)	98 (*S*)
E214W/T215S	98 (*R*)	96 (*S*)	98 (*S*)
E214I/T215S/S237A (ISA)	99 (*R*)	>99 (*S*)	>99 (*S*)
E214Y/T215S/S237A	99 (*R*)	>99 (*S*)	>99 (*S*)

Table 3
Enantioselectivity of combinatorial mutants with (*R*)-selectivity toward **1a, 5a**, and **6a**.

Mutant	*e.e.* [%]/(*R*/*S*)		
	1a	5a	6a
F161V/S196G	6 (*R*)	63 (*R*)	11 (*S*)
S196G/E214G	53 (*S*)	96 (*R*)	70 (*R*)
E214G/S237C	73 (*S*)	92 (*R*)	95 (*R*)
F161V/S196G/E214G (VGG)	86 (*S*)	99 (*R*)	98 (*R*)
S196G/E214G/S237C	80 (*S*)	98 (*R*)	79 (*R*)
Q136N/S196G/E214G	51 (*S*)	95 (*R*)	94 (*R*)

values of ISA were 0.77 mM and 4.07 s^{-1}, representing increased binding affinity and decreased catalytic efficiency. Both T215S and S237A contribute to the increased binding affinity toward **6a**, with K_M values of 0.52 mM and 1.05 mM. However, the k_{cat} values of T215S and S237A were 6.26 s^{-1} and 3.68 s^{-1}, lower than 7.29 s^{-1} of WT. It is worth noting that the k_{cat}/K_M of ISA was 5.29 $s^{-1}{\cdot}mM^{-1}$, higher than 4.58 $s^{-1}{\cdot}mM^{-1}$ of WT.

3.6. Interaction analysis of KpADH and mutants toward bulky-bulky ketones

To understand the molecular basis of stereo-preference of *Kp*ADH and mutants, molecular docking and molecular dynamic simulations were performed (Fig. 3). In the WT, substrate **1a** could be well accommodated in the active center with π-π stacking and alkyl-π interactions (Fig. 3**A**), which agrees with the high activity. With regard to **5a**, a collision was observed between CF_3-group and the side chain of E214 and Q136 (Fig. 3**B**), which is not favorable for the stabilization of **5a** in the active center. Hence, the WT displayed low activity and enantioselectivity toward **5a**. Mutation of Glu at 214 into Gly (E214G) spared more space and eliminated the unfavorable electrostatic interactions for substrate binding. Compared with WT, both binding affinity and catalytic efficiency of E214G increased to some extent. And the k_{cat}/K_M of E214G was 21.5-fold of WT (Table 4). Due to the different electrostatic and steric properties of **6a** compared with **1a, 6a** was accommodated in

Table 4
Kinetic parameters of *Kp*ADH mutants toward **5a** and **6a.**

Variant	5a			6a		
	K_M [mM]	k_{cat} [s^{-1}]	k_{cat}/K_M [s^{-1}·mM^{-1}]	K_M [mM]	k_{cat} [s^{-1}]	k_{cat}/K_M [s^{-1}·mM^{-1}]
WT	0.44±0.08	1.04±0.08	2.41	1.59±0.42	7.29±0.46	4.58
VGG	0.46±0.13	1.18±0.16	2.57	1.59±0.19	9.81±0.60	6.17
F161V	0.24±0.06	0.39±0.03	1.60	0.45±0.06	2.81±0.14	6.24
S196G	0.66±0.18	1.34±0.19	2.04	1.25±0.16	1.88±0.36	1.52
E214G	0.05±0.01	2.44±0.07	51.8	0.65±0.05	9.72±2.09	15.0
F161V/S196G	0.46±0.01	0.85±0.01	1.84	0.74±0.11	7.21±0.04	9.88
S196G/E214G	1.31±0.37	3.82±0.71	2.92	1.42±0.44	7.00±1.13	4.93
ISA	0.75±0.16	1.00±0.16	1.34	0.77±0.28	4.07±0.58	5.29
E214I	0.66±0.12	2.54±0.17	3.85	0.73±0.07	5.16±0.36	7.07
T215S	0.07±0.02	0.41±0.02	5.80	0.52±0.09	6.26±0.48	12.0
S237A	0.84±0.11	2.76±0.20	3.28	1.05±0.05	3.68±0.07	3.50
E214I/T215S	0.12±0.01	0.36±0.01	3.03	0.42±0.03	3.31±0.08	7.88
E214I/S237A	0.62±0.13	1.09±0.04	3.21	0.91±0.09	6.02±0.25	6.62

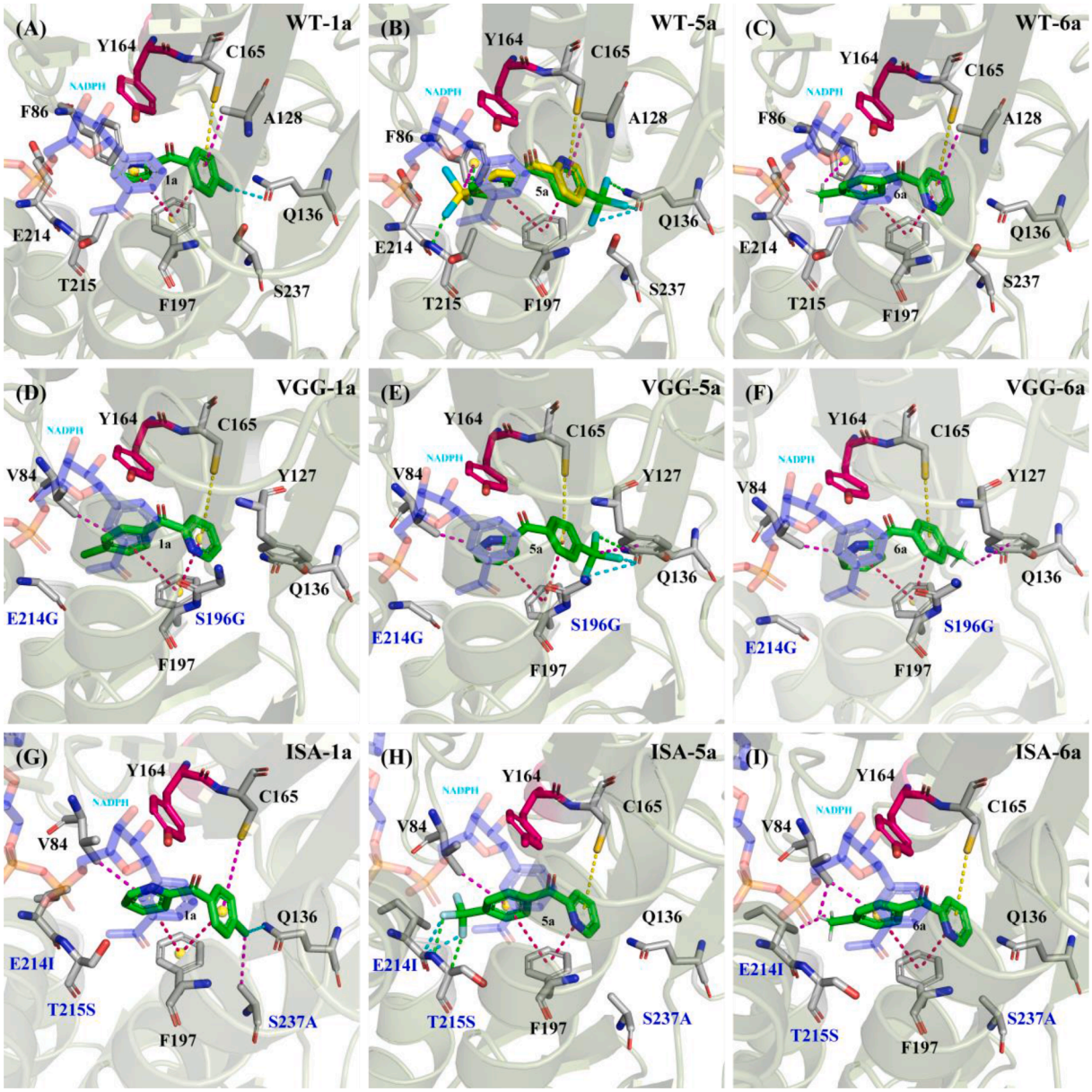

Fig. 3. Interaction analysis of **1a, 5a**, and **6a** with residues in the active center of WT, VGG, and ISA. (A) WT-**1a**, (B) WT-**5a**, (C) WT-**6a**, (D) VGG-**1a**, (E) VGG-**5a**, (F) VGG-**6a**, (G) ISA-**1a**, (H) ISA-**5a**, (I) ISA-**6a**. Residues and substrates were depicted in stick. Cyan: catalytic tyrosine (Y164), green: substrates **1a, 5a**, and **6a**, grey: residues in the active center.

the active center with different conformation because of the π-alkyl interaction between CH_3-group and F86, while **1a** was stabilized through halogen interaction between Cl-group and Q136 (Fig. 3C). In VGG, the conformation of Q136 was pushed away by Y127, which broke the interaction between the Cl-group of **1a** and Q136 (Fig. 3D). Compared with WT, substrates **5a** and **6a** were stabilized in the active center of VGG in completely inverted conformations, attributing to the expanded substrate binding pocket and enhanced interactions, including π-alkyl interaction with Y127 and the halogen interaction between Q136 and CF_3-group of **5a** (Fig. 3E & 3F). More interactions were observed with **5a** than **6a**, which agrees with the higher substrate binding affinity of **5a**. In ISA, the binding affinity of **1a** was enhanced by increased interaction between Cl-group and A237 (Fig. 3G). Furthermore, mutation of Ser at 237 into Ala spared more space for CF_3-group, which eliminated the side chain collisions and led to increased stereoselectivity. A similar role was also observed in T215S, which eliminated the collision of the pyridine group. Consequently, ISA displayed excellent stereoselectivity of >99% (*S*) toward **5a** and **6a** (Fig. 3H & 3I).

4. Conclusion

In summary, substrate specificity results revealed that the stereoselectivity of *Kp*ADH was significantly influenced by substituents at *para* position of phenyl in diaryl ketones. Two important residues, E214 and T215, were identified from single-point mutation analysis. Mutation of E214 into hydrophobic residues was favorable for (*S*)-selectivity, while hydrophilic mutation was favorable for (*R*)-selectivity. Both hydrophilic and hydrophobic mutations at T215 resulted in (*R*)-selectivity. Two stereocomplementary mutants, E214I/T215S/S237A (ISA) and F161V/S196G/E214G (VGG), were successfully constructed through combinatorial mutagenesis. The *e.e.* values of ISA and VGG toward **5a** were >99% (*S*) and 99% (*R*) respectively. Interaction analysis further demonstrated that eliminated side chain collision was beneficial for the (*S*)-selectivity of **5a** and **6a** and reversed stereoselectivity toward **1a** of ISA, while the enlarged active center and enhanced electrostatic interaction were vital for (*R*)-selectivity of VGG toward **5a** and **6a**. The study also provides guidance for the engineering of homologous carbonyl reductases for improved activity and stereoselectivity toward bulky-bulky substrates with functional substituents.

CRediT authorship contribution statement

Jiacheng Zhang: Conceptualization, Methodology, Investigation, Visualization, Writing – original draft. **Jieyu Zhou:** Resources, Methodology, Visualization. **Guochao Xu:** Resources, Writing – review & editing. **Ye Ni:** Resources, Supervision, Writing – review & editing.

Declaration of Competing Interest

The authors declare that they have no known competing financial interests or personal relationships that could have appeared to influence the work reported in this paper.

Acknowledgments

We are grateful to the National Key Research and Development Program (2021YFC2102700), the National Natural Science Foundation of China (22077054, 22078127), National First-Class Discipline Program of Light Industry Technology and Engineering (LITE2018-07), and Program of Introducing Talents of Discipline to Universities (111-2-06) for the financial support of this research.

Supplementary materials

Supplementary material associated with this article can be found, in the online version, at doi:10.1016/j.mcat.2022.112315.

References

[1] F. Hollmann, D.J. Opperman, C.E. Paul, Biocatalytic reduction reactions from a chemist's perspective, Angew. Chem. Int. Edit. 60 (11) (2021) 5644–5665, https://doi.org/10.1002/anie.202001876.
[2] J. Zhou, G. Xu, Y. Ni, Stereochemistry in asymmetric reduction of bulky-bulky ketones by alcohol dehydrogenases, ACS Catal. 10 (19) (2020) 10954–10966, https://doi.org/10.1021/acscatal.0c02646.
[3] G.-C. Xu, Y. Ni, Bioreductive preparation of ACE inhibitors precursor (*R*)-2-hydroxy-4-phenylbutanoate esters: Recent advances and future perspectives, Bioresources and Bioprocessing 2 (1) (2015), https://doi.org/10.1186/s40643-015-0040-1.
[4] Z.X. Wang, X.F. Wu, Z.N. Li, Z.D. Huang, F. Chen, Ketoreductase catalyzed stereoselective bioreduction of alpha-nitro ketones, Org. Biomol. Chem. 17 (14) (2019) 3575–3580, https://doi.org/10.1039/c9ob00051h.
[5] M. Voss, R. Kung, T. Hayashi, M. Jonczyk, M. Niklaus, H. Iding, D. Wetzl, R. Buller, Multi-faceted set-up of a diverse ketoreductase library enables the synthesis of pharmaceutically-relevant secondary alcohols, ChemCatChem 13 (6) (2021) 1538–1545, https://doi.org/10.1002/cctc.202001871.
[6] P.T. Bandeira, V. Gotor-Fernandez, L. Piovan, Stereoselective bioreduction of telluro-acetophenones to optically active hydroxy tellurides, Eur. J. Org. Chem. 2020 (9) (2020) 1129–1135, https://doi.org/10.1002/ejoc.201901841.
[7] S. Broussy, R.W. Cheloha, D.B. Berkowitz, Enantioselective, ketoreductase-based entry into pharmaceutical building blocks: ethanol as tunable nicotinamide reductant, Org. Lett. 11 (2) (2009) 305–308, https://doi.org/10.1021/ol802464g.
[8] A. Cuetos, A. Rioz-Martinez, F.R. Bisogno, B. Grischek, I. Lavandera, G. de Gonzalo, W. Kroutil, V. Gotor, Access to enantiopure alpha-alkyl-beta-hydroxy esters through dynamic kinetic resolutions employing purified/overexpressed alcohol dehydrogenases, Adv. Synth. Catal. 354 (9) (2012) 1743–1749, https://doi.org/10.1002/adsc.201200139.
[9] P. Liang, B. Qin, M. Mu, X. Zhang, X. Jia, S. You, Prelog and anti-prelog stereoselectivity of two ketoreductases from *Candida glabrata*, Biotechnol. Lett. 35 (9) (2013) 1469–1473, https://doi.org/10.1007/s10529-013-1228-0.
[10] E. Brenna, F.G. Gatti, D. Monti, F. Parmeggiani, A. Sacchetti, J. Valoti, Substrate-engineering approach to the stereoselective chemo-multienzymatic cascade synthesis of Nicotiana tabacum lactone, J. Mol. Catal. B-Enzym. 114 (2015) 77–85, https://doi.org/10.1016/j.molcatb.2014.12.011.
[11] S. Shah, R. Agera, P. Sharma, A.V. Sunder, H. Bajwa, H.M. James, R.P. Gaikaiwari, P.P. Wangikar, Development of biotransformation process for asymmetric reduction with novel anti-Prelog NADH-dependent alcohol dehydrogenases, Process Biochem. 70 (2018) 71–78, https://doi.org/10.1016/j.procbio.2018.04.016.
[12] Y.C. He, Z.C. Tao, Y. Ding, D.P. Zhang, Y.Q. Wu, Y. Lu, F. Liu, Y.F. Xue, C. Wang, J. H. Xu, Effective biosynthesis of ethyl (R)-4-chloro-3-hydroxybutanoate by supplementation of L-glutamine, D-xylose and beta-cyclodextrin in n-butyl acetate-water media, J. Biotechnol. 203 (2015) 62–67, https://doi.org/10.1016/j.jbiotec.2015.03.011.
[13] Z.Q. Liu, J.J. Ye, Z.Y. Shen, H.B. Hong, J.B. Yan, Y. Lin, Z.X. Chen, Y.G. Zheng, Y. C. Shen, Upscale production of ethyl (*S*)-4-chloro-3-hydroxybutanoate by using carbonyl reductase coupled with glucose dehydrogenase in aqueous-organic solvent system, Appl. Microbiol. Biot. 99 (5) (2015) 2119–2129, https://doi.org/10.1007/s00253-014-6245-y.
[14] J. Pan, G.W. Zheng, Q. Ye, J.H. Xu, Optimization and scale-up of a bioreduction process for preparation of ethyl (*S*)-4-chloro-3-hydroxybutanoate, Org. Process Res. Dev. 18 (7) (2014) 739–743, https://doi.org/10.1021/op500205w, 919–919.
[15] K. Wu, Z.J. Yang, X.G. Meng, R. Chen, J.K. Huang, L. Shao, Engineering an alcohol dehydrogenase with enhanced activity and stereoselectivity toward diaryl ketones: reduction of steric hindrance and change of the stereocontrol element, Catal. Sci. Technol. 10 (6) (2020) 1650–1660, https://doi.org/10.1039/c9cy02444a.
[16] L.W. Huang, J.B. Zhu, G.J. Jiao, Z. Wang, X.X. Yu, W.P. Deng, W.J. Tang, Highly enantioselective rhodium-catalyzed addition of arylboroxines to simple aryl ketones: Efficient synthesis of Escitalopram, Angew. Chem. Int. Ed. 55 (14) (2016) 4527–4531, https://doi.org/10.1002/anie.201600979.
[17] J.X. Xu, S.Y. Zhou, Y.J. Zhao, J. Xia, X.Y. Liu, J.M. Xu, B.F. He, B. Wu, J.F. Zhang, Asymmetric whole-cell bioreduction of sterically bulky 2-benzoylpyridine derivatives in aqueous hydrophilic ionic liquid media, Chem. Eng. J. 316 (2017) 919–927, https://doi.org/10.1016/j.cej.2017.02.028.
[18] A. Pennacchio, V. Sannino, G. Sorrentino, M. Rossi, C.A. Raia, L. Esposito, Biochemical and structural characterization of recombinant short-chain NAD(H)-dependent dehydrogenase/reductase from *Sulfolobus acidocaldarius* highly enantioselective on diaryl diketone benzil, Appl. Microbiol. Biotechnol. 97 (9) (2013) 3949–3964, https://doi.org/10.1007/s00253-012-4273-z.
[19] K. Wu, J.R. Yan, X.J. Wang, X.A. Yin, G.X. Shi, L. Yang, F.L. Li, J.H. Huang, L. Shao, Efficient synthesis of bepotastine and cloperastine intermediates using engineered alcohol dehydrogenase with a hydrophobic pocket, Appl. Microbiol. Biotechnol. 105 (14-15) (2021) 5873–5882, https://doi.org/10.1007/s00253-021-11413-9.
[20] J.Y. Zhou, Y. Wang, G.C. Xu, L. Wu, R.Z. Han, U. Schwaneberg, Y.J. Rao, Y.L. Zhao, J.H. Zhou, Y. Ni, Structural insight into enantioselective inversion of an alcohol dehydrogenase reveals a "Polar gate" in stereorecognition of diaryl ketones, J. Am. Chem. Soc. 140 (39) (2018) 12645–12654, https://doi.org/10.1021/jacs.8b08640.
[21] Z.T. Sun, R. Lonsdale, A. Ilie, G.Y. Li, J.H. Zhou, M.T. Reetz, Catalytic asymmetric reduction of difficult-to-reduce ketones: Triple-code saturation mutagenesis of an alcohol dehydrogenase, ACS Catal. 6 (3) (2016) 1598–1605, https://doi.org/10.1021/acscatal.5b02752.
[22] G.C. Xu, Y. Wang, M.H. Tang, J.Y. Zhou, J. Zhao, R.Z. Han, Y. Ni, Hydroclassified combinatorial saturation mutagenesis: Reshaping substrate binding pockets of

*Kp*ADH for enantioselective reduction of bulky-bulky ketones, ACS Catal. 8 (9) (2018) 8336–8345, https://doi.org/10.1021/acscatal.8b02286.

[23] G. Qu, Y.X. Bi, B.B. Liu, J.K. Li, X. Han, W.D. Liu, Y.Y. Jiang, Z.M. Qin, Z.T. Sun, Unlocking the stereoselectivity and substrate acceptance of enzymes: Proline-induced loop engineering test, Angew. Chem. Int. Ed. 61 (2022), e202110793, https://doi.org/10.1002/anie.202110793.

[24] J.Y. Zhou, G.C. Xu, R.Z. Han, J.J. Dong, W.G. Zhang, R.Z. Zhang, Y. Ni, Carbonyl group-dependent high-throughput screening and enzymatic characterization of diaromatic ketone reductase, Catal. Sci. Technol. 6 (16) (2016) 6320–6327, https://doi.org/10.1039/c6cy00922k.

[25] Y. Wang, W. Dai, Y.M. Liu, Z.W. Zhang, J.Y. Zhou, G.C. Xu, Y. Ni, Fine tuning the enantioselectivity and substrate specificity of alcohol dehydrogenase from *Kluyveromyces polysporus* by single residue at 237, Catal. Commun. 108 (2018) 1–6, https://doi.org/10.1016/j.catcom.2018.01.012.

[26] G.C. Xu, C. Zhu, A.T. Li, Y. Ni, R.Z. Han, J.Y. Zhou, Y. Ni, Engineering an alcohol dehydrogenase for balancing kinetics in NADPH regeneration with 1,4-butanediol as a cosubstrate, ACS Sustain. Chem. Eng. 7 (18) (2019) 15706–15714, https://doi.org/10.1021/acssuschemeng.9b03879.

[27] G.C. Xu, L.L. Zhang, Y. Ni, Enzymatic preparation of D-phenyllactic acid at high space-time yield with a novel phenylpyruvate reductase identified from *Lactobacillus* sp CGMCC 9967, J. Biotechnol. 222 (2016) 29–37, https://doi.org/10.1016/j.jbiotec.2015.12.011.

[28] A.A. Koesoema, D.M. Standley, S. Ohshima, M. Tamura, T. Matsuda, Control of enantioselectivity in the enzymatic reduction of halogenated acetophenone analogs by substituent positions and sizes, Tetrahedron Lett. 61 (18) (2020), https://doi.org/10.1016/j.tetlet.2020.151820.